

# MIGRATION VELOCITY ANALYSIS WITH DIFFRACTION EVENTS USING RESIDUAL MOVEOUT: APPLICATION TO SIGSBEE 2B DATA

T.A. Coimbra, J.J.S. de Figueiredo, J. Schleicher, A. Novais, and J.C. Costa

**email:** *tgo.coimbra@gmail.com and jadsomjose@gmail.com*

**keywords:** *Diffraction imaging, remigration trajectories, velocity analysis*

## ABSTRACT

*Diffraction events contain more direct information on the medium velocity than reflection events. In this work, we discuss the application of a method for migration velocity improvement and diffraction localization based on a moveout analysis of over- or undermigrated diffraction events in the depth domain. The method uses an approximate initial velocity model as input. It diffraction locations in the depth domain and information about the average velocity model which can be converted to interval velocities. The algorithm is based on the focusing of remigration trajectories from incorrectly migrated diffraction curves. The starting points of the trajectories are obtained from fitting an ellipse or hyperbola to the picked uncollapsed diffraction events in the depth-migrated domain. Focusing of the remigration trajectories points out the approximate location of the associated diffractor, as well as local velocity attributes. Apart from the migration needed at each iteration, the method has a very low computational cost, but relies on the identification and picking of uncollapsed diffractions. We demonstrate the feasibility of the method using synthetic data examples from three simple constant-gradient models and the Sigsbee2B data. While in the latter example, we were able to build a complete velocity model, we think of our technique as one for local velocity updating of a slightly incorrect model. Our example is meant to demonstrate that within regions where the assumptions are satisfied, the method can be a powerful tool.*

## INTRODUCTION

Correctly identified diffraction events in seismic data can be useful for a multitude of purposes, some of which are hydrocarbon trap indication, velocity analysis and superresolution analysis. Therefore, great effort has been made in seismic processing to improve focusing and positioning of diffractor images. Discontinuities in the subsurface (deep or shallow) can cause anomalies in seismic reflection events. A way to detect their presence is by identifying diffraction curves in the data, because the latter are typical signatures of such discontinuities. More importantly, diffraction patterns may serve as indicators of hydrocarbon traps as well as of abandoned buried targets near the surface (Zeng and McMechan, 1997).

Because of these characteristics, diffractions have since long been a subject of study in seismic methods (Krey, 1952; Kunz, 1960; Hubral, 1975). Using the focusing properties of incorrectly migrated diffractions, de Vries and Berkhout (1984) developed a technique to extract velocity information based on a minimum-entropy criterion. Several other methods to image diffractions have been proposed in the recent past (Khaidukov et al., 2004; Moser and Howard, 2008; de Figueiredo et al., 2011, 2012). Khaidukov et al. (2004) also investigate the consequences of diffraction imaging on seismic resolution. Moser and Howard (2008) proposed two approaches to diffraction imaging. One is based on reflection focusing followed by a reflection filtering, and the other is a reverse application of aperture restrictions to Kirchhoff migration in order to filter out the specular reflections and consequently to enhance diffractions. Both approaches were

applied in the depth domain. More recently, de Figueiredo et al. (2011, 2012) have developed a method for automatic detection of diffraction points based on a k-nearest-neighbour (kNN) pattern-recognition method and the diffraction operator (Tabti et al., 2004) in the time domain.

Apart from their presence signaling discontinuities in the subsurface, diffraction events are useful in another important way, this being velocity analysis by collapsing diffraction signatures. In this context, Sava et al. (2005), Novais et al. (2008), Landa and Reshef (2009) and Reshef and Landa (2009) have proposed different approaches to extract the velocity information contained in diffractions. In the cited papers, the velocity extracted by diffraction analysis was used for the purpose of migrating seismic reflectors. However, to correctly locate a reflector in the subsurface, the migration velocity used in seismic processing needs to be as close as possible to the correct velocity of the reflector overburden. Conventional seismic processing (i.e., common-midpoint analysis) is limited to NMO velocities and cannot always provide velocities of sufficient quality. More sophisticated techniques like tomography or migration velocity analysis are still expensive and may still miss important details. Therefore, the development of new techniques capable of improving the velocity model is still desirable. One such tool was presented in last year's WIT report (Coimbra et al., 2011).

Their method for diffraction-point imaging and local migration velocity improvement is based on the localization and picking of residual moveout of incorrectly migrated diffraction events in the depth domain. The analysis is formulated for execution on diffraction moveout curves in depth-migrated zero-offset (ZO) profiles. At low computational cost, the method uses an approximate velocity model as an input and provides an update to the velocity. The algorithm of using residual diffraction moveout for velocity updating is based on depth remigration (Hubral et al., 1996a; Tygel et al., 1996; Hubral et al., 1996b; Schleicher et al., 1997, 2004) and gives rise to a new method for diffraction localization that relies on the picking of over- or undermigrated diffractions in the image. In this work, we demonstrate the feasibility of this method on a collection of numerical examples, including the SIGSBEE 2B data. It should be noted that the proposed technique can be applied simultaneously with residual-moveout-based migration velocity analysis.

## RESIDUAL DIFFRACTION MOVEOUT

In this section, we briefly summarize the method for diffraction fitting and velocity updating. For more details, the reader is referred to last year's WIT report of Coimbra et al. (2011).

### Theoretical description

Let us consider a diffraction point at the true position  $(x_t, z_t)$  in a constant-velocity medium with true velocity  $v_t$ . From the underlying arguments of depth remigration (Hubral et al., 1996b), it follows that the residual moveout of a diffraction event after depth migration with a wrong velocity  $v_0$  is nothing else than the corresponding Huygens image-wave for depth remigration from velocity  $v_t$  to  $v_0$  (both  $v_0$  and  $v_t$  assumed to be constant). According to Hubral et al. (1996b), the location of the Huygens image-wave is the curve or surface of all points where a possible (reflection or diffraction) event at an image point  $(x, z)$  might be placed when the migration velocity is changed from  $v_t$  to  $v_0$ . Since a diffraction event migrated with the true velocity  $v_t$  focuses at the true position  $(x_t, z_t)$ , its location after migration with a wrong velocity  $v_0$  is smeared over the location of the Huygens image-wave, which can be written as an ellipse or hyperbola (Coimbra et al., 2011),

$$\frac{z^2}{b^2} + s \frac{(x - x_t)^2}{a^2} = 1, \quad (1)$$

depending on the sign  $s = \text{sgn}(v_0^2 - v_t^2) = \text{sgn}(v_0 - v_t)$  of the difference between the true and migration velocities. The half-axes  $a$  and  $b$  are given by

$$a = \frac{z_t}{v_t} \sqrt{|v_0^2 - v_t^2|} \quad \text{and} \quad b = \frac{z_t}{v_t} v_0. \quad (2)$$

As we can see from equation (1) when the migration velocity is smaller than the medium velocity, the undermigrated diffraction event follows a hyperbola. On the other hand, when the migration velocity is higher than the medium velocity, the overmigrated diffraction event follows an ellipse.

### Residual moveout detection

Of course, the above expressions are exact only for a constant-velocity medium. Under the assumptions that (1) the model is sufficiently correct above the region where the diffractions are found so that overburden effects are corrected for by migration, (2) the velocity variations in that region are moderate so that wave propagation can be described locally by a constant average velocity, and (3) local velocity errors affect diffractions only locally, we expect equation (1) to still approximately describe incorrectly migrated diffractions in a heterogeneous medium.

Whenever the local velocity distribution at the diffraction point satisfies the above conditions reasonably well, we can use the theoretical description in equation (1) to pick the incorrectly migrated diffraction event. We use the least-squares method to find the best-fitting hyperbola to describe an undermigrated diffraction event or the best-fitting ellipse for an overmigrated diffraction event. This provides estimates for the half-axes  $a$  and  $b$  as well as for horizontal coordinate of the apex,  $x_t$ . The process depends on the size of the aperture in which the hyperbolas or ellipses are fitted to the migrated diffraction event. In our implementation, we started with a large aperture and reduced in small steps it until further reduction did no longer affect the least-squares residual.

Incorrectly migrated diffraction events in an environment with a very strong velocity gradient exhibit a strong tilt. For a better description of the residual moveout in this case, we modify equation (1). We use a mixed perturbation term  $\varepsilon(x - x_t)z$  to allow for a rotation of the ellipse or hyperbola, i.e., equation 1 becomes

$$\frac{z^2}{b^2} + s \frac{(x - x_t)^2}{a^2} = 1 + \varepsilon(x - x_t)z, \quad (3)$$

The perturbation parameter  $\varepsilon$  is adjusted together with the other parameters of the ellipse or hyperbola in the least-squares procedure. Since its only purpose is to improve the fit, the value of  $\varepsilon$  is not used in the further procedure.

## VELOCITY UPDATING

After identification, picking and fitting, the residual moveout of the incorrectly migrated diffraction events can then be used to update the migration velocity model. Coimbra et al. (2011) described two different ways of how the so-obtained information can be used for the purpose of velocity updating. The first consists of inverting the half-axes  $a$  and  $b$  of the fitted ellipses or hyperbolas for  $v_t$  and  $z_t$  using equations (2). The second traces the remigration trajectories, that is, the set of positions where a selected reflection point can be found in a migrated image as a function of migration velocity. Note that, as proven by Liptow and Hubral (1995) and Schleicher et al. (1997) from geometrical considerations, the remigration trajectories in the depth domain are actually circular arcs. At  $v = v_t$ , they focus at the true diffraction point. Thus, the focusing property can be used to determine a velocity estimate. In the implementation used in this work, we employed the procedure using the trajectory-tracing system. It traces remigration trajectories starting at each of the fitted ellipses or hyperbolas. The velocity at which the remigration trajectories focus define the local (average) velocity, which is then attributed to the focus point in the updated model.

### Model building

As mentioned before, the theoretical description above was derived for constant velocity. To be of use in practice, it must be applicable in inhomogeneous media, and the velocity information extracted from identified diffraction events must be used to build an inhomogeneous velocity model. Under the three assumptions detailed above, local velocity information can be extracted if one or several incompletely migrated diffraction events are located in a vicinity that can be described by a small number of velocity parameters. In such vicinities, we proceed in the way illustrated in Figure 1. If there is only a single diffraction event in a certain region of interest, we can determine one diffractor location and the local average velocity (Figure 1a). From two diffraction events in the region, we can determine two diffractor locations, one local average velocity and the one component of the velocity gradient. This component can be calculated for a previously known preferential direction, e.g., the vertical gradient assuming horizontal homogeneity, or else in the direction between the two estimated diffractor locations (Figure 1b). In our examples in this work, we chose to assume horizontal homogeneity and estimate an approximate vertical

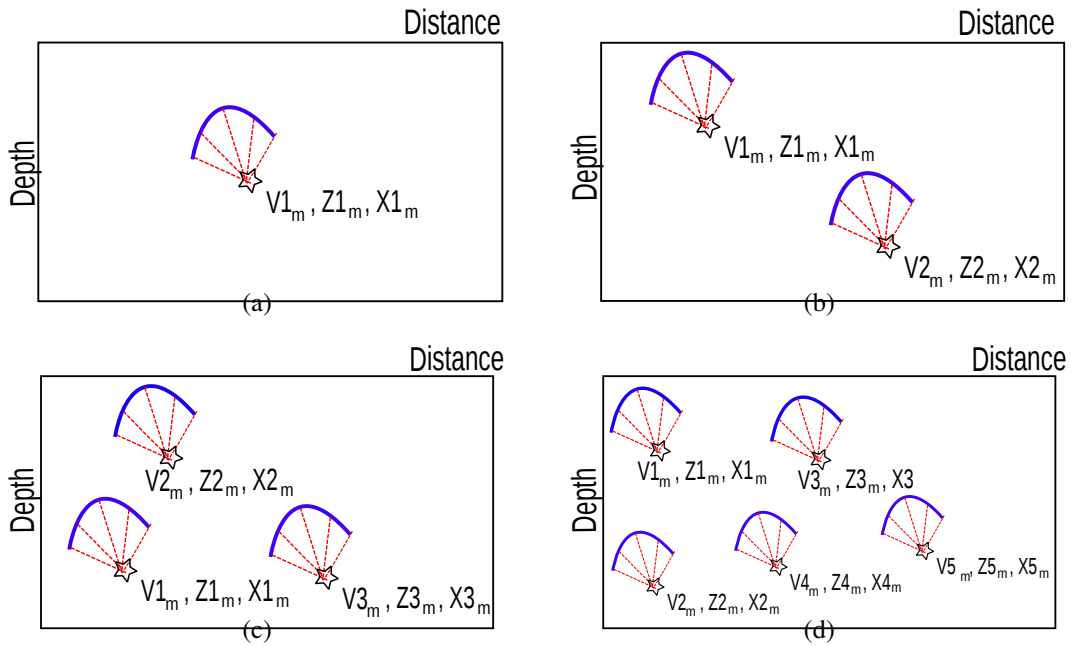


**Figure 1:** Velocity model building from remigration trajectory focusing in dependence of the number of diffraction events available within a region of interest. (a) One event; (b) two events; (c) three events; (d) more than three events. For details, see text.

component. If we have three diffraction events at our disposal, we can obtain three diffractor locations, one local average velocity and both the horizontal and vertical gradient components (Figure 1c). If there are more than three diffraction points in the region of interest, we estimate all diffractor locations, one local average velocity and two gradient components using a least-squares fit (Figure 1d).

Velocities outside the considered region containing the used diffractions are considered known for the purpose of velocity model building. If velocities at points close to the diffraction region are known, they are used to improve the estimates of the local gradients, for instance near the sea bottom in the SIGSBEE example below.

The resulting velocity parameters are then interpolated in order to find an average velocity model. This model has then to be inverted for interval velocities. As experimentally shown by Schleicher et al. (2004), the average velocity governing depth remigration in medium with vertical velocity variations only corresponds to the slowness average over the interval velocities. The average velocity  $V_m(z)$  between two depth levels  $z_0$  and  $z$  is given by the formula

$$\frac{1}{V_m(z)} = \frac{1}{z - z_0} \int_{z_0}^z \frac{dZ}{V_r(Z)}, \quad (4)$$

where  $V_r(Z)$  is the true medium interval velocity at depth  $Z$ . Depth  $z_0$  is the last depth of the overburden where the velocity model is considered correct, i.e., the depth level where the current region of interest begins.

Equation (4) can be inverted for interval velocity as

$$\frac{1}{V_r(z)} = \frac{d}{dz} \left( \frac{z - z_0}{V_m(z)} \right). \quad (5)$$

We use equation (5) irrespectively of possible horizontal variations in the model to invert our average velocity models for interval velocity. The procedure is as follows. We use equation (4) to convert the present interval-velocity model to vertical average velocities, trace the remigration trajectories to determine the average-velocity updates, correct those values accordingly, and convert the corrected values back to

interval velocities using formula (5). Improvements could be made by integrating along ray trajectories instead of the vertical axis.

After model building, a new migration step is required to evaluate the quality of the resulting interval velocity model. If the considered diffraction events are not collapsed, or if new uncollapsed diffraction events become visible and interpretable, the method is applied again. This process continues iteratively until all visible and interpretable diffractions are sufficiently well collapsed.

## NUMERICAL EXAMPLES

We have applied our velocity updating technique to three simple constant-gradient velocity models and the more complex Sigsbee2B data set. In the constant-gradient models, we have reduced the number of available diffractions in comparison to Coimbra et al. (2011).

### Constant velocity gradient

The first two models consist of a single diffraction point buried in a model with a constant velocity gradient in the vertical and horizontal directions, respectively, given by  $v(z) = 2000 + 0.5z$  m/s and  $v(x) = 2000 + 0.5x$  m/s (see Figure 2a and b). The corresponding synthetic datasets were generated by Kirchhoff modeling (see Figure 2c and d), simulating a zero-offset section with 200 source-receivers pairs spaced at 10 m and covering an extension of 2000 m for both models. We used a Ricker wavelet of dominant frequency 25 Hz. To these synthetic data we added random noise with a signal-to-noise ratio (S/N) of 10 with respect to the strongest part of the diffraction event.

We then migrated the resulting seismic sections using a wrong constant velocity model of 2000 m/s with the depth migration Gaussian Beam code of SU for the zero offset configuration (Cohen and Stockwell, 2006). Figures 2e and f show the resulting migrated section. Of course, the diffractions are not focused in the migrated image. Since the migration velocity is smaller than the true medium velocity, all diffractions are undermigrated. To these undermigrated diffraction events, we applied the remigration-trajectories method. First, we fitted hyperbolic arcs to the events (blue lines in Figures 2e and f). Starting from these arcs, we traced the remigration trajectories using the tracing system of Coimbra et al. (2011) (red lines). The black dots indicate the focusing points of the trajectories, which coincide within 1% with the true locations of the diffractors, demonstrating that even for a nonconstant velocity, trajectory focusing locates the diffractors with acceptable precision.

Under the assumption of a known velocity of 2000 m/s at the top left corner of the model, our method found  $V_r(z) = 2000 + 0.53z$  m/s for the vertical-gradient model and  $V_r(x) = 2000 + 0.49x$  m/s for the horizontal-gradient model. This is equivalent to a gradient error of 6% in the first case and of 2% in the second case. In both cases, the method needed only a single iteration to come up with a reasonable velocity model and an acceptably focused diffractor. Note that in a corresponding experiment with a too high migration velocity (not shown here) the focusing of the remigration trajectories occurred in the same way and the velocity extraction was of the same quality.

In order to investigate the influence of an unknown gradient direction, we applied our method to a slightly more complex model (see Figure 3a). It contains three diffractor points buried in a constant-gradient velocity background with vertical and lateral variation, given by  $v(x, z) = 2000 + 0.5z + 0.5x$  m/s. Again, we generated zero-offset data by Kirchhoff modeling with the same modeling parameters as before. These zero-offset data are depicted in Figure 3b. The migration of these data was performed using the same Gaussian beam operator as before. Figure 3c shows depth migrated image using a constant velocity of 2000 m/s.

By applying the remigration-trajectories method, the trajectories (see the red lines in Figure 3c) from the diffraction curves focus exactly at the true depths. In this example, even under a rather strong lateral and vertical velocity gradient, the method was capable of localizing all diffraction points with an error of  $\pm 0.5\%$  in the vertical direction and up to  $\pm 1.0\%$  in the horizontal direction. Using the three velocity values extracted at the three points, we determined an average velocity model given by  $V_m(x, z) = 2050 + 0.51x + 0.3z$  m/s. Conversion to an interval velocity model using equation (4), results in  $V_r(x, z) = 2050 + 0.51x + 0.5z$  m/s (see Figure 3d). This corresponds to an error of about 2.5% for the initial velocity, and 2% for the horizontal gradient. The vertical gradient is estimated exactly within the limits

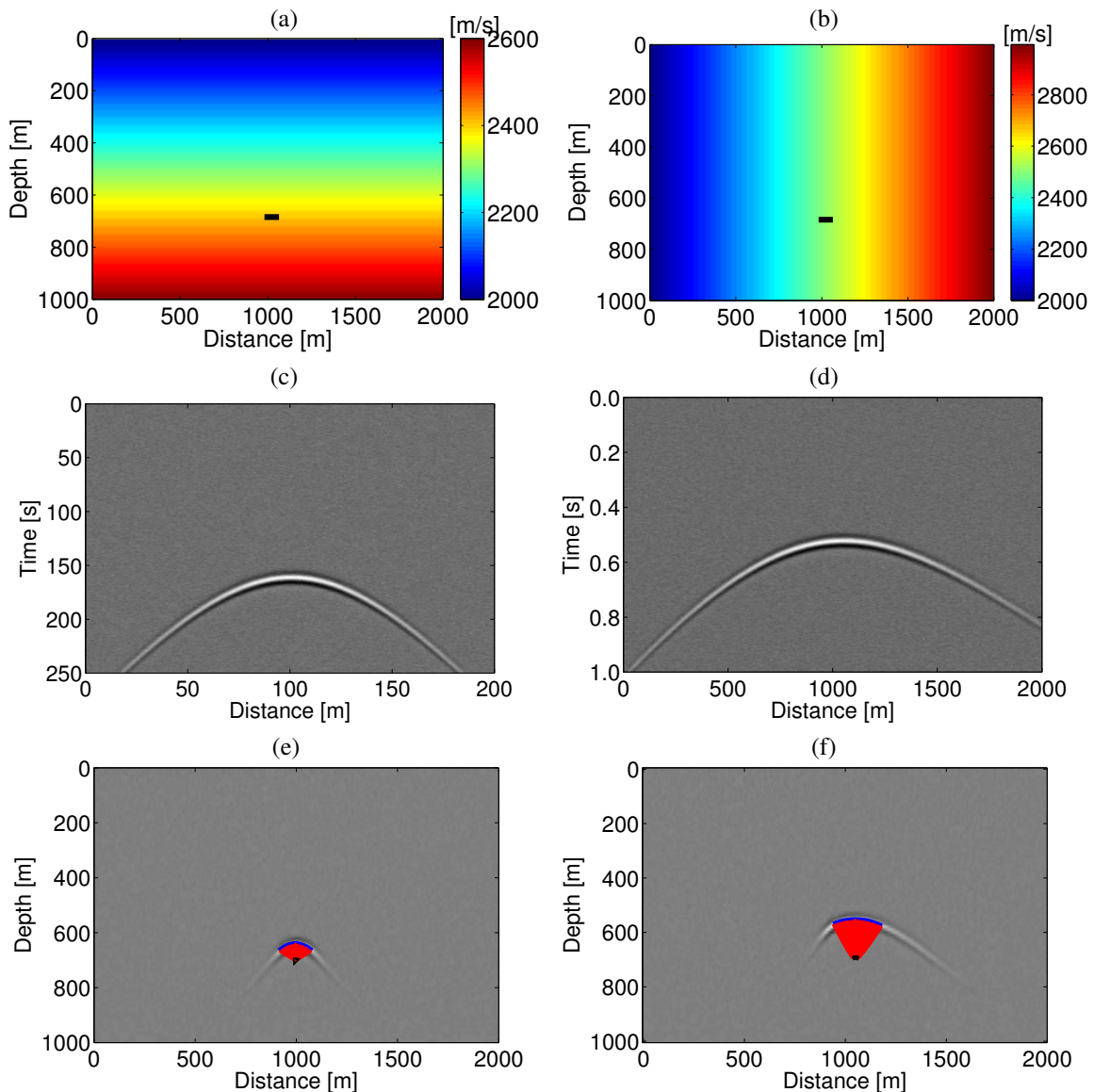


**Figure 2:** Remigration trajectory focusing for two constant-gradient models with a single diffractor buried at 700 m depth. (a) Model with vertical gradient  $v(z) = 2000 + 0.5z$  m/s. (b) Model with horizontal gradient  $v(x) = 2000 + 0.5x$ . (c) and (d) Zero-offset time sections over models in (a) and (b). (e) and (f) Undermigrated hyperbolas (blue lines) and focusing remigration trajectories (red lines) for models in (a) and (b).

of computational precision. This leads to very small overall errors in the constructed velocity model. Figure 3e shows the relative velocity error with respect to the true velocity model depicted in Figure 3a. Note that the largest velocity error in the top right corner is less than 2%.

Using this velocity model, we migrated the data depicted in Figure 3b. The result can be seen in Figure 3f. As can be noted, all diffractor points are nicely collapsed at their correct positions (compare to model in Figure 3a). In the same way as for the vertical and horizontal gradient models with a known initial velocity, the method needed only a single iteration to find an acceptable velocity model.

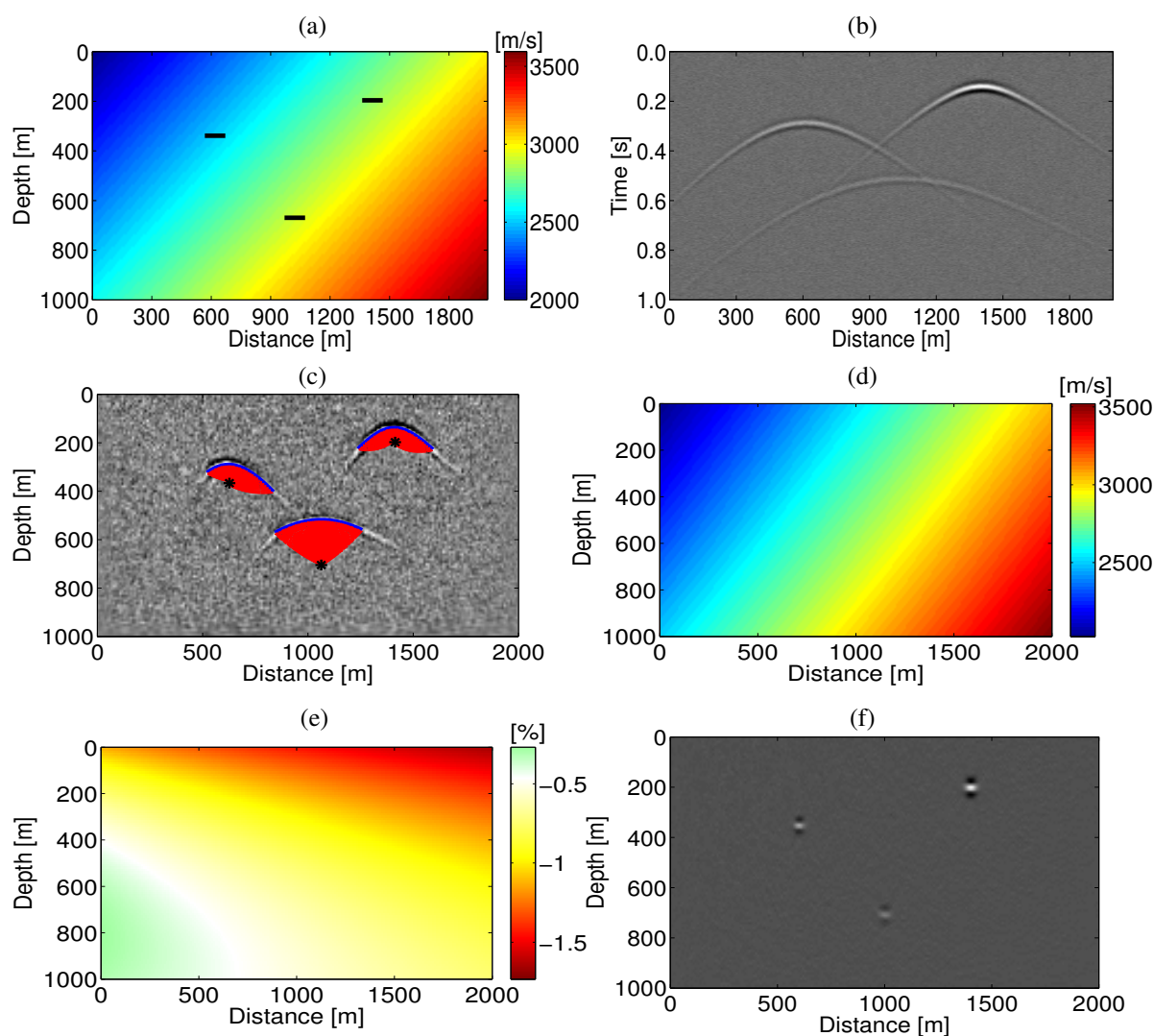


**Figure 3:** Constant-gradient model with  $v(z) = 2000 + 0.5x + 0.5z$  m/s, containing three diffractor points. (b) Zero-offset dataset generated by Kirchhoff modeling. (c) Depth migrated image with constant velocity of 2000 m/s. Also shown are the picked hyperbolic arcs of the undermigrated diffraction events (blue lines) and the remigration trajectories collapsing at the correct depth points (red lines). (d) Reconstructed interval velocity model with  $V_r(z) = 2050 + 0.51x + 0.5z$  m/s. (e) Relative velocity error. (f) Migrated image using the velocity model of (d).

### Sigsbee2B data

For a test under more realistic conditions, we applied our method to the Sigsbee2B data. We chose the Sigsbee model (see Figure 4a) because of the explicitly present diffraction points, and because the Sigsbee background model is very well approximated in large parts by a constant-gradient medium, which makes our local concepts valid over broader ranges, thus requiring less diffraction events. This made a full velocity analysis possible, without the need for a sophisticated starting model. The zero-offset data section is depicted in Figure 4b. It consists of 496 traces recorded with source-receiver pairs separated by 45.75 m. The total recording time of each trace is 8 s and the number of samples per trace is 1001, resulting in a time sample rating of 0.008 s.

We started with a zero-offset depth migration with a constant velocity of 1500 m/s using SU's Gaussian beam migration (see Figure 4c). Note that in practice, a short-offset section should suffice to start the

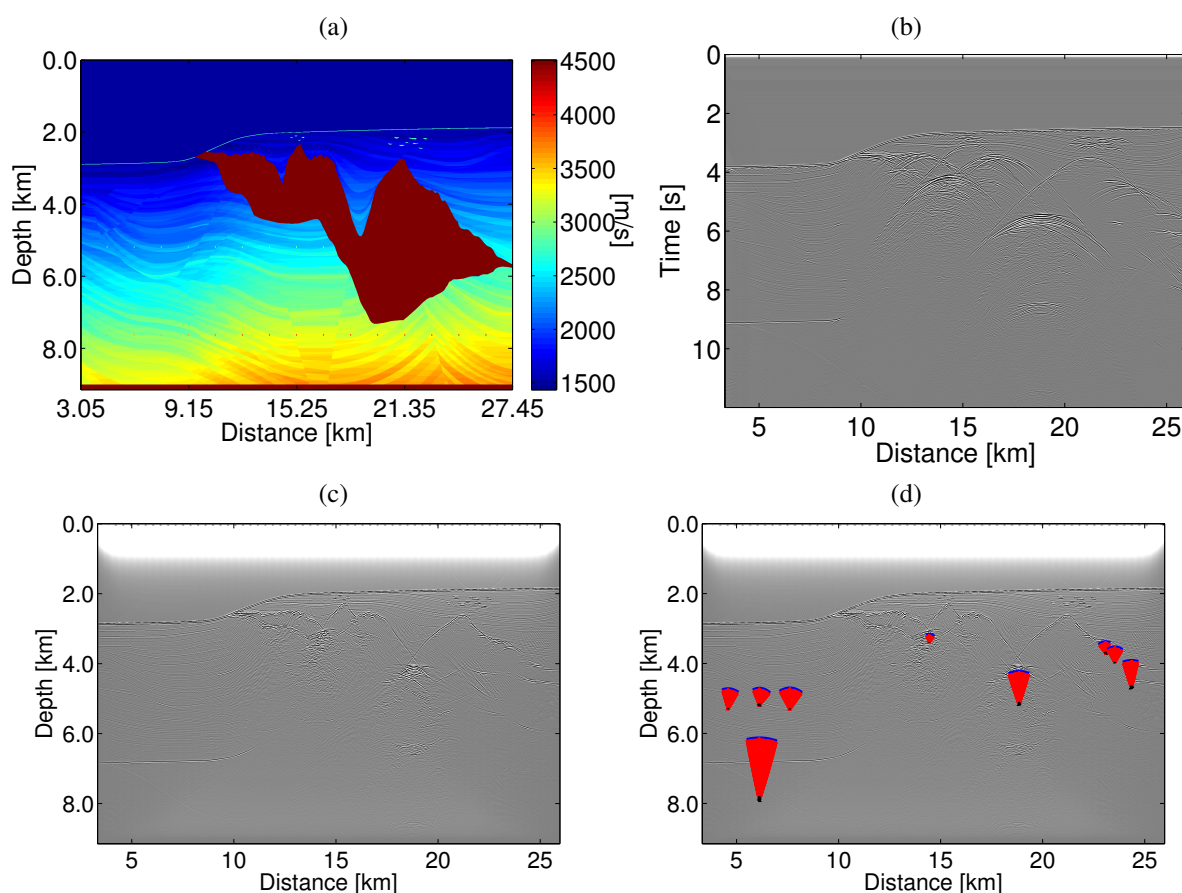


**Figure 4:** (a) Stratigraphic Sigsbee velocity model. (b) Zero-offset time section. (c) Gaussian-beam migrated section for initial constant velocity of 1500 m/s. (d) Migrated section together with remigration trajectories (red lines) for nine selected diffractions curves.

iterations. In this first migrated image, only the sea bottom comes into focus. We selected some easily detectable undermigrated diffractions and picked their uncollapsed diffraction curves (in blue). We then traced the corresponding remigration trajectories (shown as red lines in Figure 4d) emanating from the incorrectly migrated diffraction events. For each diffraction event, the resulting remigration trajectories are focusing in a single point, which can be considered a first guess for the true position of the diffractor. The focus points of the remigration trajectories also provide estimates for the local velocity.

Initially we applied our method using nine uncollapsed diffraction events. Each following iteration used less events. These were mostly still uncollapsed diffraction events that had already been used in the previous iterations and a very small number of newly interpretable diffractions. After four iterations, the velocity model obtained with our method was good enough to collapse the diffractor points located at the left side in the Sigsbee model (see Figure 4a). After the fifth iteration using a total of 26 diffraction events, we reached the interval velocity model shown in Figure 5a. The resulting Gaussian-beam depth migrated section can be seen in Figure 5b.

We decided to stop the process after 5 iterations because down to the top-of-salt reflector, the resulting image is of very high quality (see Figure 5b). Even the very deep salt trough at the center of the image has been nicely resolved and correctly positioned. As shown in Figure 5b, the top of salt and the prominent sediment reflectors were imaged with a positioning error of less than 1%. It must be stressed that even in a model as large as the Sigsbee model, our method was effectively fast and of a very low computational cost.

Figure 6 compares a selected part from the left side of the image of Figure 5a to the corresponding part of the sedimentary region in the stratigraphic velocity model (Figure 6b). We see that the method was capable of placing all diffraction points at their correct position with an error as small as  $\pm 0.1$  km in the

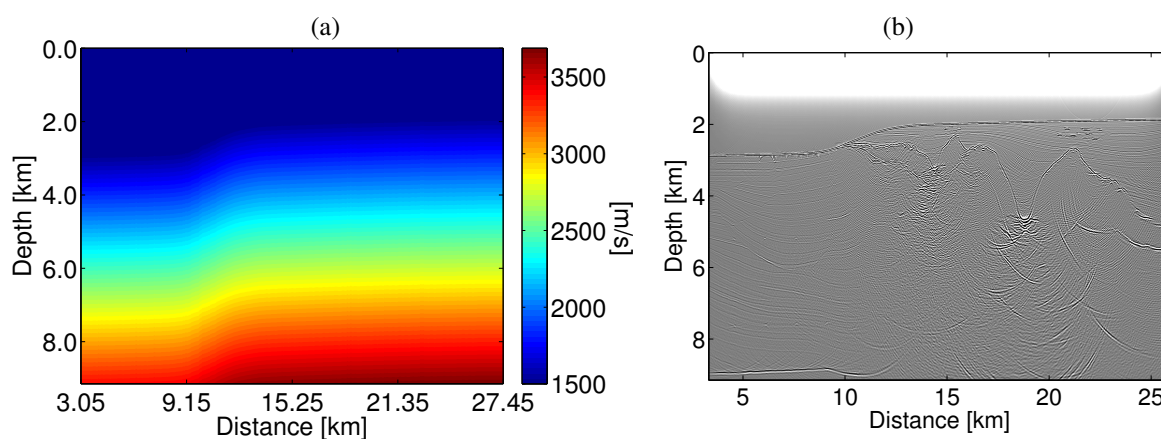


**Figure 5:** (a) Velocity model after fifth and final iteration. (b) Migrated section using velocity model in (a).

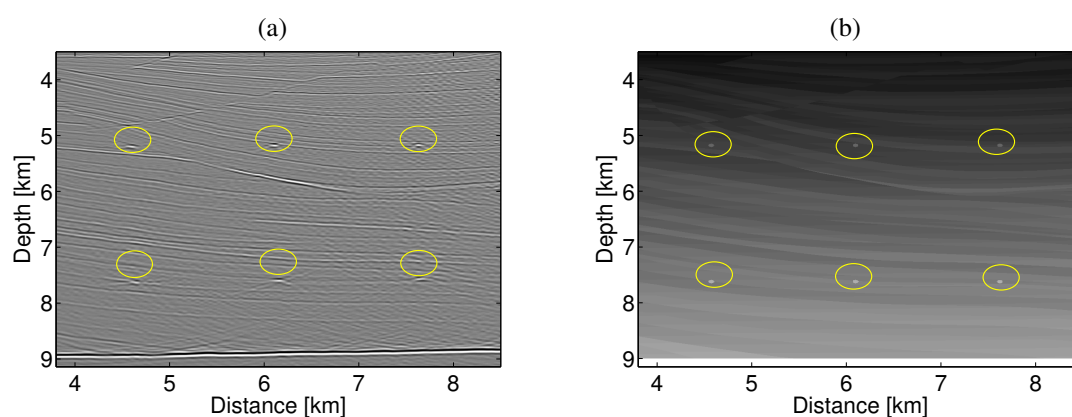


**Figure 6:** (a) Section of migrated section from Figure 5b. (b) Section of stratigraphic model from Figure 4a.

lateral direction and an even smaller error in the vertical direction. Note that the position of the normal fault in Figure 6a was already almost perfect after the first iteration. Thus, we conclude that the method can provide very accurate velocity information in complex layered media.

It is important to note that in this case a very small number of identified and picked diffractions in a range of one to five iterations was sufficient to estimate a very good velocity model. Using only nine diffraction curves in the first iteration, and a total of 26 diffractions in all iterations together, we were capable of producing a high-quality image of the sedimentary region in the Sigsbee model. This demonstrates that in regions where incorrectly migrated diffraction events can be identified, the method is able to extract reliable velocity information that can be used to update the initial model.

It is worth mentioning here that the repositioning using remigration trajectories can also be applied to reflection events. In this case, the remigration trajectories will point out where the image would be located for any other average migration velocity. Thus, at points, where the true depth of a reflector is known, e.g., at well positions, the method can also be employed to update the velocity model.

### Subsalt imaging

In order to complete the imaging of the Sigsbee2B data, we continued our processing with the following steps. We next picked the top-of-salt reflector in Figure 5b and flooded the model below it with salt velocity 4514 m/s (see Figure 7a). The increased complexity of the model did no longer allow for the use

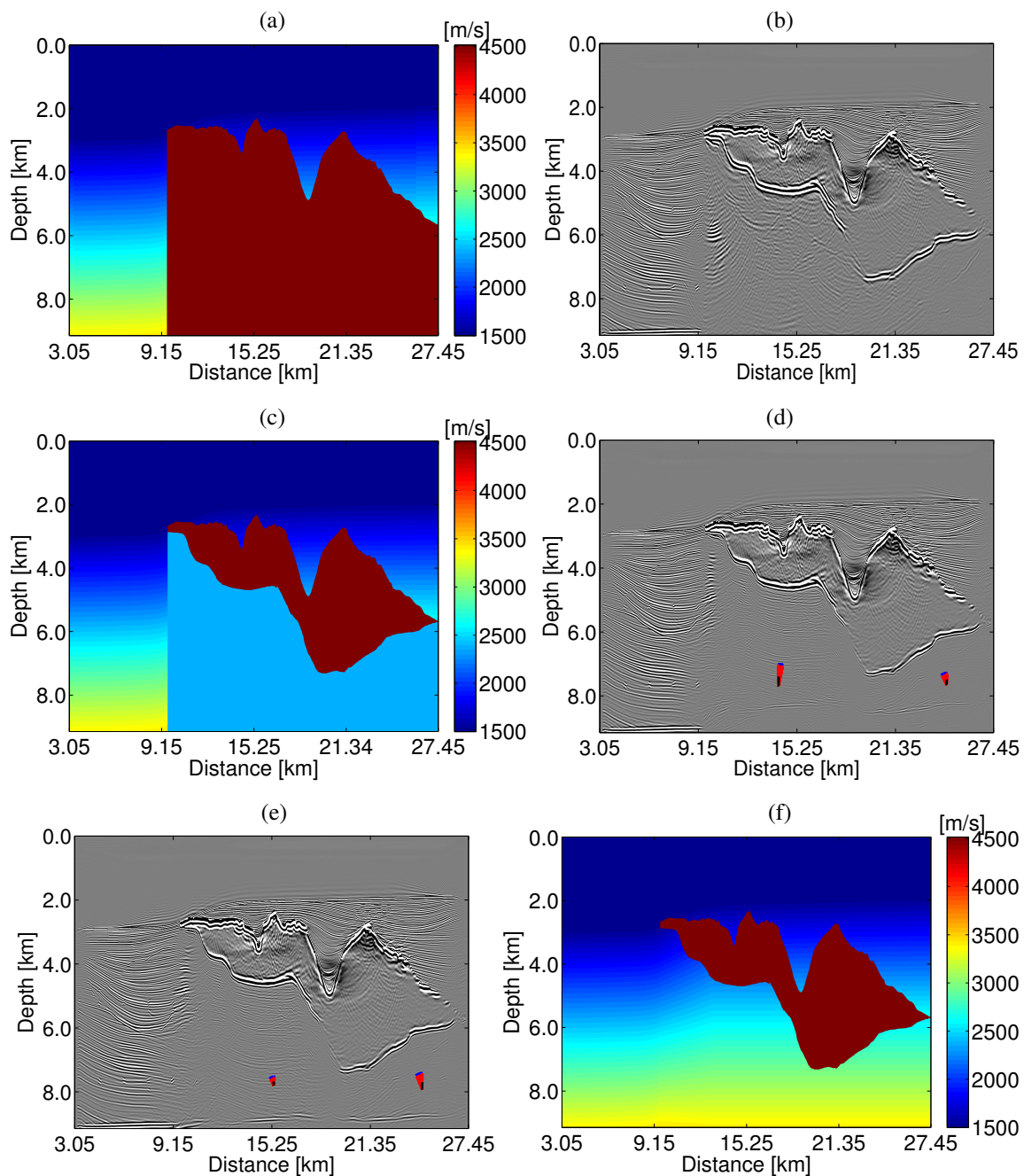


**Figure 7:** (a) Velocity model after salt flooding. (b) Migrated section using the velocity model after salt flooding. (c) Velocity model after bottom-of-salt picking and sediment flooding. (d) Migrated section using the velocity model in (c) together with remigration trajectories (red lines). (e) Migrated section using the velocity model after last-but-one iteration together with remigration trajectories (red lines). (f) Velocity model after the final iteration.

of the Gaussian beam zero-offset migration, but required a more robust algorithm. Thus, we employed the prestack complex Padé FD one-way wave-equation migration operator developed by Amazonas et al. (2007) to 496 shots separated by 45.72 m. All sources and receivers are located at 7.62 m from the water surface.

In the resulting stacked image (see Figure 7b), we could then pick the salt bottom, below which we

flooded the model with sediment velocity. In order to be able to test our method, we chose the sediment velocity of 2380 m/s, found in the model of Figure 5a at the deepest part in the top-salt trough for the flooding (Figure 7c). In a first test, we had used the velocities from the model of Figure 5a below the salt. This resulted in a too perfect focusing of the subsalt diffractors for our purposes, since no further velocity updating was required.

Using the model of Figure 7c, we employed the same prestack migration as before to obtain the image shown in Figure 7d. This image allowed to identify two diffraction events suited for our analysis. After two more iterations, one with only a single event, and one with the two events shown in Figure 7e, we reached our final model depicted in Figure 7f. In the transition zone between 9.20 km and 13.0 km, where no velocity information was available, we used linear interpolation between the two neighboring regions to complete the model. A comparison with the stratigraphic Sigsbee model (Figure 4a) reveals a very great similarity, indicating the high quality of the so-derived velocity model.

Finally, we migrated the Sigsbee2B data using the true-amplitude extension of the complex Padé FD migration (Amazonas et al., 2010) for using the velocity model of Figure 7f and with the reference velocity model for the Sigsbee2B data, provided by SMAART-JV. The two migrated sections are depicted in Figures 8a and b, respectively. The velocity model produced by our approach provides an image with the correct stratigraphic location of sedimentary layers as well as correct positioning and imaging of almost all diffractor points. Even in the subsalt region, our result reaches almost the quality of the one obtained with the reference velocity field.

The model of Figure 7f and image of Figure 8a had to be considered final because there are no diffraction events with an elliptic or hyperbolic shape in the image. However, some of the subsalt diffractors are visible but clearly unfocused, and do not present an interpretable shape. This points towards velocity errors in the overburden rather than the local velocity. This could be a reason to reexamine the picking of the salt body for further improvements.

It is worth mentioning that in this paper, we have made no effort to increase the number of visible uncollapsed diffractors, since the number of identifiable diffraction events was sufficient to build a reasonable velocity model. However, if the number of visible diffraction events is limited, there are methods which can highlight diffraction events that are hidden behind stronger reflection energy (Moser and Howard, 2008; Bansal and Imhof, 2005; Melo et al., 2009), separate reflection and diffraction events (Fomel et al., 2007), or even generate diffraction signatures from reflector events (Santos et al., 2010, 2012).

## CONCLUSIONS

We have tested the method for diffraction imaging and velocity model improvement in the depth domain proposed in last year's WIT report by Coimbra et al. (2011). The method uses the moveout of unfocused diffraction events in a migrated seismic section. It relies on the assumption that for an acceptable overburden velocity, unmigrated diffraction events are predominantly determined by the local velocity error and can thus be approximately described by elliptic or hyperbolic arcs. Conversely, the presence in the image of unfocused diffractors that do not follow these arcs points toward velocity errors in the overburden.

The behavior of detected diffraction events that approximately follow these elliptic or hyperbolic arcs under variation of the local migration velocity can be described by remigration trajectories (also called velocity rays). The focusing of the remigration trajectories originating from these events is used to determine the correct location of the diffractor and the associated velocity value. The methodology does not require any information apart from an initial velocity model for an initial depth migration. In our numerical examples, this model needed not be close to the true velocity distribution. In other situations, more accurate initial models might be required. Certainly, a good model is required for the region above any available diffraction events. The processing time of the method between migrations is very fast. Once the diffraction events are Selected and picked, the necessary computations are executed in a matter of seconds.

We have tested the technique in three simple constant-gradient models, one in the vertical, one in the horizontal and one in the diagonal direction. In all three examples, the method has worked satisfactorily. It has positioned all diffraction points with an error of less than 1%. The extracted velocity models were acceptably accurate, with an error of less than 2% in the regions where the diffractors were located. In a fourth, more realistic numerical example using the Sigsbee2B data set, after five iterations using altogether 26 diffraction events, the method produced a velocity model that was capable of correctly imaging

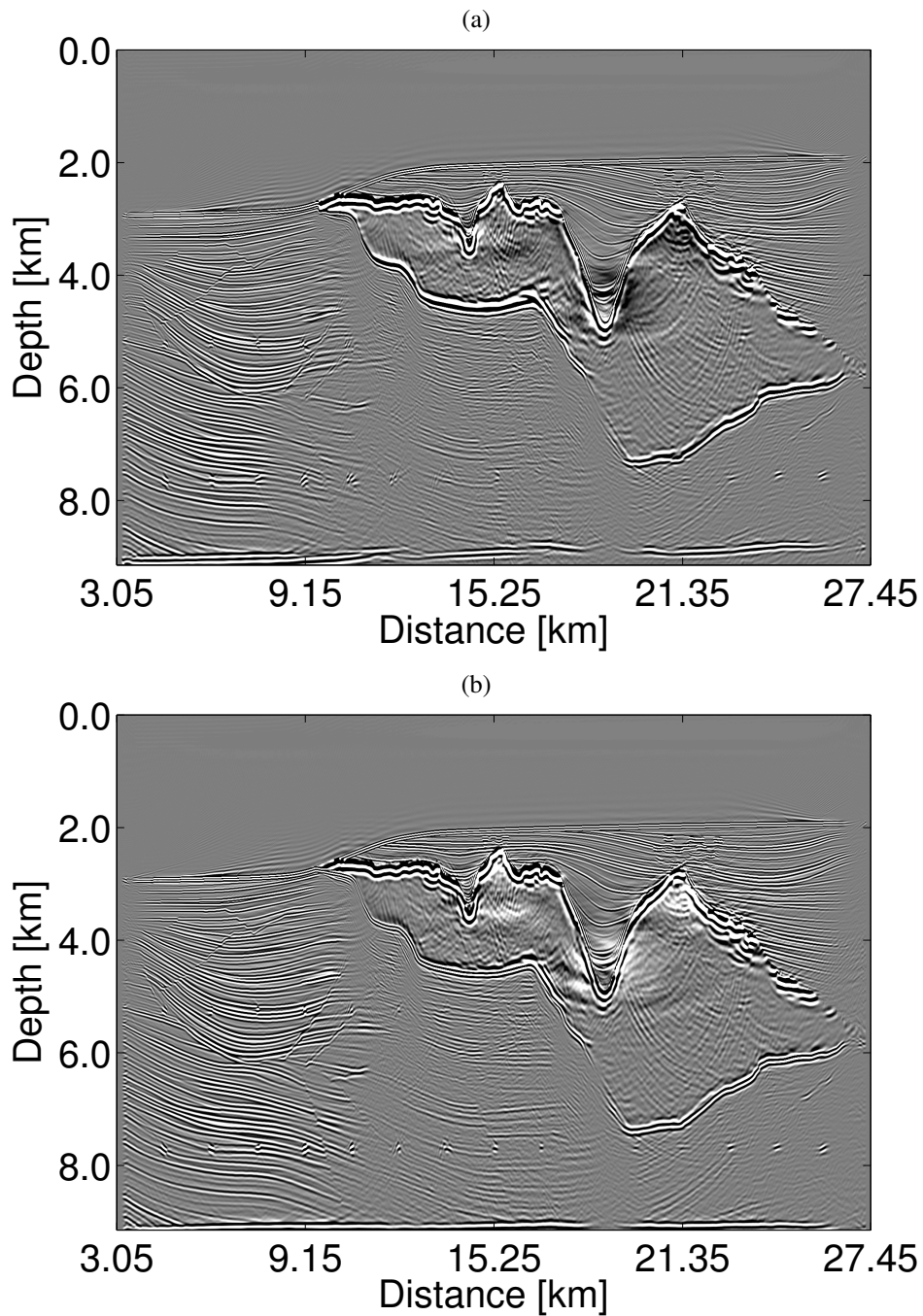


**Figure 8:** Prestack true-amplitude complex Padé FD migration of the Sigsbee 2B data using (a) the velocity model of Figure 7f, (b) the Sigsbee reference velocity model for migration (from the SMAART-JV repository).

the sedimentary region between the sea bottom and the top of salt reflectors. After top-of-salt picking, salt flooding, and bottom-of-salt picking, another three iterations were sufficient to produce an acceptable subsalt velocity model.

Note, however, that full velocity building from scratch was possible in this example because of the rather simple background model of the Sigsbee data. The practical applicability of the method in more complex models and under more realistic conditions, particularly with respect to picking diffractions in

2D and 3D, in the presence of coherent and incoherent noise, requires further research. It is expected that for more complex models, more diffractions in different regions of the model will be necessary to achieve convergence at an acceptable velocity model. If few diffraction events are available, only local velocity improvements can be expected.

### ACKNOWLEDGEMENTS

The authors thank SMAART-JV for providing the Sigsbee2B data and model. This work was kindly supported by the Brazilian agencies CAPES, FINEP, and CNPq, as well as Petrobras and the sponsors of the *Wave Inversion Technology (WIT) Consortium*.

### REFERENCES

- Amazonas, D., R. Aleixo, G. Melo, J. Schleicher, A. Novais, and J. Costa, 2010, Including lateral velocity variations in true-amplitude common-shot wave-equation migration: *Geophysics*, **75**, S175–S186.
- Amazonas, D., J. Costa, J. Schleicher, and R. Pestana, 2007, Wide angle FD and FFD migration using complex Padé approximations: *Geophysics*, **72**, S215–S220.
- Bansal, R., and M. G. Imhof, 2005, Diffraction enhancement in prestack seismic data: *Geophysics*, **70**, V73–V79.
- Cohen, J. K., and J. W. Stockwell, Jr., 2006, CWP/SU: Seismic Un\*x release no. 39: A free package for seismic research and processing: Center for Wave Phenomena, Colorado School of Mines.
- Coimbra, T. A., J. J. S. de Figueiredo, A. Novais, and J. Schleicher, 2011, Migration velocity analysis with diffraction events using residual moveout: *Annual WIT Report*, **15**, no. 5, 57–70.
- de Figueiredo, J. J. S., F. Oliveira, E. Esmi, L. Freitas, S. Green, A. Novais, and J. Schleicher, 2011, Diffraction imaging point of common-offset gather: GPR data example: 81st Ann. Internat. Meeting, SEG, Expanded Abstracts, 4339–4343.
- de Figueiredo, J. J. S., F. Oliveira, E. Esmi, L. Freitas, J. Schleicher, A. Novais, P. Sussner, and S. Green, 2012, Automatic detection and imaging of diffraction points using pattern recognition: *Geophysical Prospecting*, **60**. (in print).
- de Vries, D., and A. J. Berkhout, 1984, Velocity analysis based on minimum entropy: *Geophysics*, **49**, 2132–2142.
- Fomel, S., E. Landa, and M. T. Taner, 2007, Poststack velocity analysis by separation and imaging of seismic diffractions: *Geophysics*, **72**, no. 6, U89–U94.
- Hubral, P., 1975, Locating constant a diffractor below plane layers of interval velocity and varying dip: *Geophysical Prospecting*, **23**, 313–322.
- Hubral, P., J. Schleicher, and M. Tygel, 1996a, A unified approach to 3-D seismic reflection imaging - Part I: Basic concepts: *Geophysics*, **61**, 742–758.
- Hubral, P., M. Tygel, and J. Schleicher, 1996b, Seismic image waves: *Geoph. J. Int.*, **125**, 431–442.
- Khaidukov, V., E. Landa, and T. J. Moser, 2004, Diffraction imaging by focusing-defocusing: An outlook on seismic superresolution: *Geophysics*, **69**, 1478–1490.
- Krey, T., 1952, The significance of diffractions in the investigation of faults: *Geophysics*, 843–858.
- Kunz, B. F. J., 1960, Diffraction problems in fault interpretation: *Geophysical Prospecting*, **8**, 381–388.
- Landa, E., and M. Reshef, 2009, Separation, imaging, and velocity analysis of seismic diffractions using migrated dip-angle gathers: 79th Ann. Internat. Meeting, SEG, Expanded Abstracts, 2176–2180.
- Liptow, F., and P. Hubral, 1995, Migrating around in circles: *The Leading Edge*, **14**, 1125–1127.
- Melo, P. E. M., M. J. Porsani, and M. G. Silva, 2009, Ground-roll attenuation using a 2D time-derivative filter: *Geophysical Prospecting*, **57**, 343–353.
- Moser, T. J., and C. B. Howard, 2008, Diffraction imaging in depth: *Geophysical Prospecting*, **56**, 627–641.
- Novais, A., J. Costa, and J. Schleicher, 2008, GPR velocity determination by image-wave remigration: *Journal of Applied Geophysics*, **65**, 65–72.
- Reshef, M., and E. Landa, 2009, Post-stack velocity analysis in the dip-angle domain using diffractions: *Geophysical Prospecting*, **57**, 811–821.
- Santos, L. A., D. M. S. Filho, A. Bulcão, C. E. Theodoro, W. J. Mansur, and G. A. McMechan, 2010, Tomographic inversion over diffraction CFP operators in structurally complex areas: SEG Denver 2010 Annual Meeting, 4275–4279.

- Santos, L. A., W. J. Mansur, and G. A. McMechan, 2012, Tomography of diffraction-based focusing operators: *Geophysics*, **77**, no. 5, R217–R225.
- Sava, P., B. Biondi, and J. Etgen, 2005, Wave-equation migration velocity analysis by focusing diffractions and reflections: *Geophysics*, **70**, U19–U27.
- Schleicher, J., P. Hubral, G. Höcht, and F. Liptow, 1997, Seismic constant-velocity remigration: *Geophysics*, **62**, 589–597.
- Schleicher, J., A. Novais, and F. P. Munerato, 2004, Migration velocity analysis by depth image-wave remigration: First results: *Geophysical Prospecting*, **52**, 559–573.
- Tabti, H., L.-J. Gelius, and T. Hellmann, 2004, Fresnel aperture prestack depth migration: *First Break*, **22**, no. 3, 39–48.
- Tygel, M., J. Schleicher, and P. Hubral, 1996, A unified approach to 3-D seismic reflection imaging - Part II: Theory: *Geophysics*, **61**, 759–775.
- Zeng, X., and G. A. McMechan, 1997, GPR characterization of buried tanks and pipes: *Geophysics*, **62**, 797–806.